

1 **Distinguishing Emission-Associated Ambient Air PM<sub>2.5</sub> Concentrations and Meteorological**  
2 **Factor-Induced Fluctuations**

3 Qirui Zhong<sup>†</sup>, Jianmin Ma<sup>†</sup>, Guofeng Shen<sup>†</sup>, Huizhong Shen<sup>†</sup>, Xi Zhu<sup>†</sup>, Xiao Yun<sup>†</sup>, Wenjun Meng<sup>†</sup>, Hefa  
4 Cheng<sup>†</sup>, Junfeng Liu<sup>†</sup>, Bengang Li<sup>†</sup>, Xilong Wang<sup>†</sup>, Eddy Y. Zeng<sup>Δ</sup>, Dabo Guan<sup>‡</sup>, Shu Tao<sup>†\*</sup>

5 <sup>†</sup> *College of Urban and Environmental Sciences, Laboratory for Earth Surface Processes, Sino-French Institute for Earth*  
6 *System Science, Peking University, Beijing 100871, China*

7 <sup>Δ</sup> *Guangdong Key Laboratory of Environmental Pollution and Health, School of Environment, Jinan University, Guangzhou*  
8 *510632, China*

9 <sup>‡</sup> *School of International Development, University of East Anglia, Norwich, Norfolk, NR4 7TJ, UK*

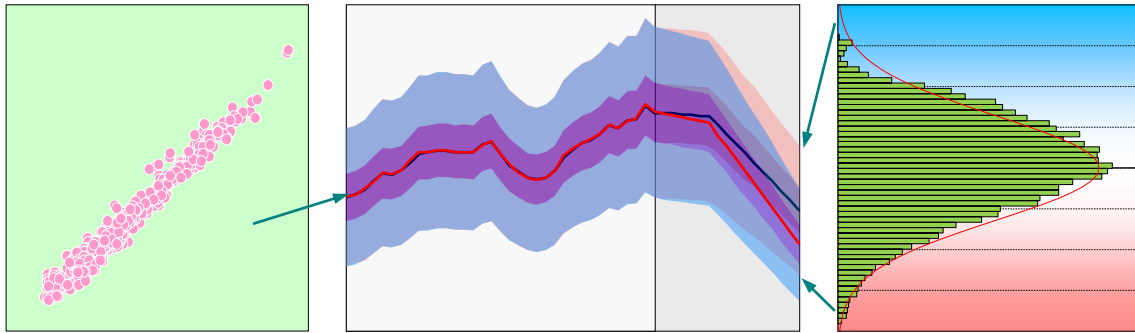
10

11

12 **Word counting:** 5865 + 1500 (5 figures) = **7365**

13

14 TOC Art



15

16

17

18 **ABSTRACT**

19 Although PM<sub>2.5</sub> (particulate matter with aerodynamic diameters of less than 2.5 μm) in the air originates  
20 from emissions, its concentrations are often affected by confounding meteorological effects. Therefore,  
21 direct comparisons of PM<sub>2.5</sub> concentrations made across two periods, which are commonly used by  
22 environmental protection administrations to measure the effectiveness of mitigation efforts, can be  
23 misleading. Here, we developed a two-step method to distinguish the significance of emissions and  
24 meteorological factors and assess the effectiveness of emission mitigation efforts. We modeled ambient  
25 PM<sub>2.5</sub> concentrations from 1980 to 2014 based on three conditional scenarios: realistic conditions, fixed  
26 emissions, and fixed meteorology. The differences found between the model outputs were analyzed to  
27 quantify the relative contributions of emissions and meteorological factors. Emission-related gridded PM<sub>2.5</sub>  
28 concentrations excluding the meteorological effects were predicted using multivariate regression models,  
29 whereas meteorological confounding effects on PM<sub>2.5</sub> fluctuations were characterized by probabilistic  
30 functions. By combining the regression models and probabilistic functions, fluctuations in the PM<sub>2.5</sub>  
31 concentrations induced by emissions and meteorological factors were quantified for all model gridcells and  
32 regions. The method was then applied to assess the historical and future trends of PM<sub>2.5</sub> concentrations and  
33 potential fluctuations on global, national, and city scales. The proposed method may thus be used to assess  
34 the effectiveness of mitigation actions.

35

## 36 INTRODUCTION

37 PM<sub>2.5</sub> (particulate matter with aerodynamic diameters of less than 2.5 μm) is a major environmental and  
38 health concern<sup>1,2</sup>. PM<sub>2.5</sub> in the air originates from the direct emissions of primary aerosols and from the  
39 secondary formation of aerosols from various precursors<sup>3</sup> and ambient PM<sub>2.5</sub> concentrations are shaped  
40 primarily by the emission rates<sup>4-6</sup>. In addition to emissions, meteorological conditions are critical to the  
41 formation and transport of PM<sub>2.5</sub> through the air<sup>7-9</sup>. Interannual climate variability can also affect regional  
42 pollution levels<sup>10</sup>. Therefore, spatiotemporal variations in PM<sub>2.5</sub> concentrations in the atmosphere are  
43 mainly driven by the combined effects of emissions, chemical reactions, and meteorology<sup>11</sup>.

44 Although the impacts of emissions and meteorological confounding effects on PM<sub>2.5</sub> pollution have been  
45 studied extensively<sup>12-14</sup>, a lack of understanding of interactions between them has often led to confusion  
46 among the public and policymakers. For example, local governments often report on the effectiveness of  
47 their mitigation efforts from observed reductions in annual mean PM<sub>2.5</sub> concentrations ignoring  
48 considerable fluctuations in meteorological conditions occurring between years. Such a practice is  
49 misleading whenever strong positive or negative meteorological interferences occur. For example, an  
50 abnormal increase in PM<sub>2.5</sub> concentrations occurred following a period of PM<sub>2.5</sub> decline in northern China  
51 in early 2017. The average PM<sub>2.5</sub> concentration in the first half-year of 2017 (66 μg/m<sup>3</sup>) was slightly higher  
52 than that during the same period in 2016 (64 μg/m<sup>3</sup>) in Beijing although comprehensive mitigation efforts  
53 have been made in recent years. The event has stimulated debate on the effectiveness of recent mitigation  
54 actions<sup>15</sup> even though these efforts have already led to a continuous decrease in annual mean PM<sub>2.5</sub>  
55 concentrations in this area in recent several years<sup>16</sup>. A recent study has suggested that the abnormal increase  
56 during the first six months of 2017 was strongly associated with anomalies in humidity.<sup>17</sup>

57 To quantify the contributions of emissions and confounding meteorological factors to ambient PM<sub>2.5</sub>  
58 concentrations, a two-step approach was developed. In brief, global PM<sub>2.5</sub> concentrations from 1980 to  
59 2014 were simulated based on three conditional modeling scenarios: 1. realistic conditions, 2. fixed  
60 meteorology (realistic daily emission estimates but fixed meteorological parameters for 2014) and 3. fixed  
61 emissions (realistic daily meteorological variables with mean emissions from 1980 to 2014). Based on the  
62 results of the simulations, regression models were developed for individual gridcells to predict  
63 emission-driven PM<sub>2.5</sub> trends. Probabilistic functions were established to characterize superimposed

64 meteorology-associated fluctuations. By combining the regression models and probabilistic function, PM<sub>2.5</sub>  
65 concentration trends to be induced by changes in emissions and meteorological factor-associated  
66 fluctuations could be distinguished. The effectiveness of emission mitigation measures could thus be  
67 evaluated. Moreover, future trends of ambient PM<sub>2.5</sub> concentrations can be predicted based on projected  
68 changes in emissions.

## 69 **METHODS**

70 **Overall Approach.** Fig. 1 shows the overall scheme of the proposed approach including 1) a simulation  
71 based on three scenarios and 2) the development of regression models and probabilistic functions.

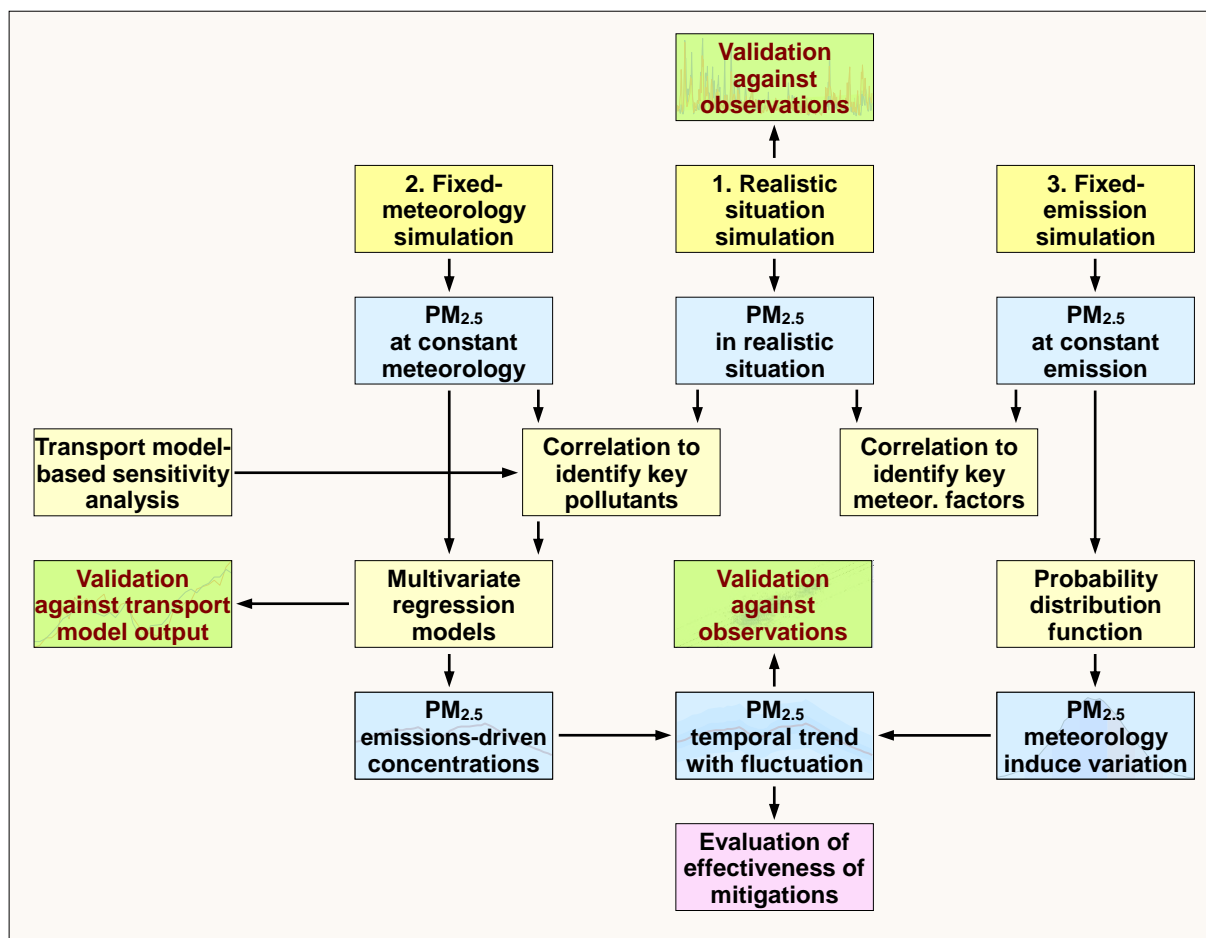


**Fig. 1** Flowchart showing the research scheme of this study. Gridded  $PM_{2.5}$  concentrations were simulated for the three scenarios from 1980 to 2014. Individual effects of emissions and meteorological factors were measured. Regression models were developed using the second model's scenario simulation output to predict gridded  $PM_{2.5}$  concentrations based on emissions. Meteorological confounding effect-induced variations were quantified as probabilistic functions using the third model's scenario simulation output. Using the models, trends in  $PM_{2.5}$  concentrations with a variability range were generated, and the effectiveness of mitigation measures were evaluated. The procedures were validated at various stages.

72

73 **Atmospheric Chemical Transport Modeling and Validation.** The MOZART4 (Model for Ozone and

74 Related Chemical Tracers, version 4) was applied to simulate daily  $PM_{2.5}$  concentrations from 1980 to 2014

75 on a global scale<sup>18</sup>. The model was set with a  $1.895^\circ$  (latitude)  $\times$   $1.875^\circ$  (longitude) horizontal resolution,

76 with 28 vertical layers, and with a 15-minute time step. The species considered include black carbon (BC),

77 organic carbon (OC), unspecified PM<sub>2.5</sub> (primary PM<sub>2.5</sub> - BC - 1.3OC), SOA (Secondary Organic Aerosol),  
78 sulfate, nitrate, ammonium, dust, and sea salt. Emissions were obtained from the PKU (Peking  
79 University)-series for primary aerosols (PM<sub>2.5</sub>, BC, and OC), SO<sub>2</sub> (sulfur dioxide) and NO<sub>x</sub> (nitrogen  
80 oxides)<sup>19</sup>. Emissions drawn from other inventories were also used in this study, including NH<sub>3</sub> and  
81 nonbiogenic NMVOC (Nonmethane Volatile Organic Carbon) data collected from EDGAR (Emissions  
82 Database for Global Atmospheric Research) and HTAPv2 (Hemispheric Transport of Air Pollution, version  
83 2)<sup>20,21</sup>, biogenic VOC (Volatile Organic Carbon) data collected from MEGAN (Model of Emissions of  
84 Gases and Aerosols from Nature)<sup>22</sup>, and open-field biomass burning emission data collected from GFED4.1  
85 (Global Fire Emissions Database, version 4.1)<sup>23</sup>. NCEP/NCAR (National Centers for Environmental  
86 Prediction/National Centers for Atmospheric Research) reanalysis products<sup>24</sup> were used as offline  
87 meteorological inputs. Aerosol optical depths from MODIS (Moderate Resolution Imaging  
88 Spectroradiometer)<sup>25</sup> were used as a proxy to downscale the model predicted parameters into a fine gridcell  
89 of 0.125°×0.125°<sup>26</sup>. Model performance was evaluated against more than 220 thousand daily monitoring  
90 data points collected from around the world (**Fig. S1**), against time series observations for six major cities  
91 around the world (**Fig. S2**), and against major components (**Fig. S3**). It can be observed that the majority of  
92 data points fall around the 1:1 line without bias and that the deviation of the predicted concentrations from  
93 the observations increase as the time scale decreases. For the annual means primarily used in this study,  
94 87% of data points are within the two-fold range.

95 **Conditional Scenarios and Relative Contributions.** The simulation was conducted based on three  
96 conditional modeling scenarios. The control run was conducted using realistic emission estimates and  
97 meteorological fields. For the fixed-meteorological condition scenario, meteorological parameters for 2014  
98 (a normal non-El Niño year) were applied to all years with realistic emission estimates data. For the  
99 fixed-emission scenario, 35-year-averaged emissions were applied to all years together with realistic  
100 meteorological conditions. Deviations in the fixed emissions and fixed meteorological condition  
101 simulations from the normal simulation (control run) were normalized to their respective fractions to  
102 quantify the overall contributions of emissions ( $RC_E$ ) and meteorological conditions ( $RC_M$ ) for a given  
103 region (from a gridcell to the globe) and for a given period (from a month to multiple years) of interest.

104 **Sensitivity Analysis.** A sensitivity analysis was conducted to identify major air pollutants governing  
105 ambient air PM<sub>2.5</sub> concentrations through a preliminary simulation for January 2010 (monthly resolution).

106 Modeling was repeatedly performed by reducing or enhancing the emissions of individual pollutants by  
107 10%, 25%, 50%, 75%, or 100% each time. The 21 pollutants tested include primary PM<sub>2.5</sub> (including  
108 primary BC, OC and unspecified PM<sub>2.5</sub>), SO<sub>2</sub>, NH<sub>3</sub>, NO<sub>x</sub>, CO, CH<sub>3</sub>SCH<sub>3</sub>, C<sub>6</sub>H<sub>5</sub>(CH<sub>3</sub>), BIGALK (lumped  
109 alkanes with C > 3), C<sub>2</sub>H<sub>4</sub>, BIGENE (lumped alkenes with C > 3), C<sub>3</sub>H<sub>6</sub>, CH<sub>2</sub>O, CH<sub>3</sub>CHO, CH<sub>3</sub>OH,  
110 CH<sub>3</sub>COCH<sub>2</sub>CH<sub>3</sub>, C<sub>3</sub>H<sub>8</sub>, C<sub>2</sub>H<sub>5</sub>OH, C<sub>2</sub>H<sub>6</sub>, CH<sub>3</sub>COCH<sub>3</sub>, C<sub>10</sub>H<sub>16</sub>, and C<sub>5</sub>H<sub>8</sub>. The results of the sensitivity  
111 analysis are listed in **Table s1**.

112 **Emission-based Regression Model.** Based on the results of the sensitivity analysis, the four main air  
113 pollutants were used for regression model development. Using annual emissions of these pollutants as  
114 independent variables and PM<sub>2.5</sub> concentrations from the fixed-meteorology simulation as a dependent  
115 variable for 35 years, multivariate regression models with both dependent and independent variables  
116 log-transformed were developed for individual gridcells to predict PM<sub>2.5</sub> concentrations without  
117 meteorological confounding effects. The regression was established for all individual gridcells using data  
118 for 35 years. The uncertainty of the regression models based on the fixed-meteorology simulation was  
119 characterized by a 90% confidence interval of predicted PM<sub>2.5</sub> concentrations. Model-predicted PM<sub>2.5</sub>  
120 concentrations were compared against those calculated from the fixed-meteorology simulation (the same  
121 data set used for model development). The method cannot be applied to model PM<sub>2.5</sub> variation on a  
122 relatively short time scale such as a daily scale, which can be affected by many occasional extreme  
123 emission or meteorological events, as well as the nonlinearity of secondary formation of aerosol.

124 **Meteorology-related Probabilistic Functions.** For each individual gridcell, the frequency distribution of  
125 the annual mean PM<sub>2.5</sub> concentrations for a 35-year period derived from the fixed-emission simulation was  
126 used as a meteorology-related probabilistic function to quantify random variations of PM<sub>2.5</sub> induced by  
127 changes in meteorology at each gridcell. The function can also be generated for a region (such as a country)  
128 at other time scales (such as a month) of interest. At 84% of all model gridcells, the probabilistic functions  
129 calculated follow a normal distribution with a zero mean (K-S test,  $p > 0.05$ ).

130 **Characterization of Emission-Driven Trends with Meteorology-Induced Fluctuations.** This was done  
131 by combining emission-based trends with meteorology-induced variations from 1980 to 2030. Using  
132 emissions and PM<sub>2.5</sub> concentrations for 2014 as baselines, the gridcell-specific models were applied to  
133 project the trajectory of PM<sub>2.5</sub> concentrations induced by given emission changes for all gridcells across the



134 globe. When superimposed on predicted  $PM_{2.5}$  concentrations derived from regression models, variations  
135 induced by fluctuations in meteorological variables presented as  $UI_{50}$  (intervals between the 25<sup>th</sup> and 75<sup>th</sup>  
136 percentiles) and  $UI_{95}$  (intervals between the 2.5<sup>th</sup> and 97.5<sup>th</sup> percentiles) were derived using the distribution  
137 pattern discussed in the previous section. Prior to future projections, combined model simulations were  
138 conducted for a period from 1988 (when the first valid observation was available) to 2014 and were  
139 validated against 2940 field observations collected from IMPROVE (Interagency Monitoring of Protected  
140 Visual Environments) for the United States and from EMEP (The European Monitoring and Evaluation  
141 Programme) for European countries at annual scale, and corresponding results are shown in **Fig. S4**.

142 **Other Analysis.** Statistical analysis was conducted using SPSS 23.0<sup>27</sup> with a significance level of 0.05.  
143 Monte Carlo simulations were performed using MATLAB R2016b<sup>28</sup> to generate the frequency distribution  
144 functions associated with variation of meteorological parameters for individual gridcells.

145 **Limitations and Uncertainties.** The methodology is affected by limitations and uncertainties. For example,  
146 the emission inventories are subject to uncertainty, and meteorological conditions for a single year (2014)  
147 are not truly representative. Like other atmospheric chemical transport models<sup>14</sup>, MOZART cannot provide  
148 model uncertainty information, while Monte Carlo simulation for complex atmospheric chemistry  
149 modeling would be unrealistic due to extremely high computation loading. Moreover, many  
150 physicochemical processes were not even included<sup>29,30</sup>. Contribution of SOA to  $PM_{2.5}$  formation is often  
151 underestimated by the modeling. To date, very limited multiple-year observation data are available on a  
152 global scale, which are critical for model validation. Last but not the least, the overall uncertainty of the  
153 two-step procedure was unable to be characterized due to the limitations listed above. Nevertheless, there is  
154 still room to further improve the method. In addition to updating the inventories, quantifications of the  
155 effects of individual pollutants and meteorological factors could help to mitigate such uncertainties.

156 **RESULTS AND DISCUSSION**

157 **Effects of Emissions and Meteorological Factors.** Based on the results of a sensitivity analysis, the  
158 relative contributions of various air pollutants to PM<sub>2.5</sub> concentrations and the responses of PM<sub>2.5</sub> to these  
159 pollutants are shown in **Fig. S5**. As is shown, 97% of the variations in PM<sub>2.5</sub> concentrations are attributable  
160 to the emission of primary PM<sub>2.5</sub> (56.9±28.6%) followed by the emission of SO<sub>2</sub> (18.9±8.8%), NH<sub>3</sub>  
161 (12.9±6.6%), and NO<sub>x</sub> (8.3±6.8%), respectively. Similar results have recently been reported<sup>31,32</sup>.  
162 Significant ( $p < 0.05$ ) correlations between the emissions of the four pollutants and PM<sub>2.5</sub> concentrations  
163 derived from the fixed-meteorology simulation were found for 70% of land gridcells around the world,  
164 denoting the feasibility of predicting emission-driven PM<sub>2.5</sub> concentrations based on emission densities of  
165 these pollutants while excluding confounding meteorological effects. Those land gridcells (30%) not  
166 showing significant correlations between pollutant emissions and ambient PM<sub>2.5</sub> concentrations were  
167 mostly identified in desert areas and high-latitude regions with low emissions, such as the Sahara Desert  
168 and the Arctic Archipelago.

169 **Fig. 2** presents maps of partial correlation coefficients between emissions and PM<sub>2.5</sub> concentrations on an  
170 annual basis. The four major pollutants in terms of their respective contribution to PM<sub>2.5</sub> concentrations,  
171 including primary PM<sub>2.5</sub>, SO<sub>2</sub>, NO<sub>x</sub>, and NH<sub>3</sub>, are shown. Primary PM<sub>2.5</sub>-dominated partial correlations  
172 were found for China and India, where coal and biomass fuels used for power generation, industry,  
173 residential sectors, and cement production are the most important emission sources<sup>33,34</sup>. In the United States,  
174 PM<sub>2.5</sub> concentrations are more SO<sub>2</sub> emission-dependent, which is consistent with the large fraction of  
175 sulfates in total PM<sub>2.5</sub> concentrations observed in the country<sup>35</sup>. For most Western European countries,  
176 primary PM<sub>2.5</sub> and SO<sub>2</sub> made a synthetic contribution to PM<sub>2.5</sub> mass concentration (such was the case in  
177 Germany<sup>36</sup>), whereas NO<sub>x</sub> has a stronger effect on France. The influence of NH<sub>3</sub> mainly occurred in  
178 Eastern European countries and Russia (west) because NH<sub>3</sub> exhausted from the agriculture sector (e.g.,  
179 fertilizer and domesticated animals) is the leading factor affecting formation of ammonium sulfate and  
180 nitrate<sup>1</sup>. The significance of the correlation increased as the time scale changed from annual to daily. For  
181 example, median correlation  $p$  values of SO<sub>2</sub> are 0.14 (0.012-0.46), 0.011 (0.0000038-0.29), and  $9.4 \times 10^{-31}$   
182 ( $3.1 \times 10^{-105}$ - $7 \times 10^{-7}$ ) on annual, monthly, and daily scales, respectively.

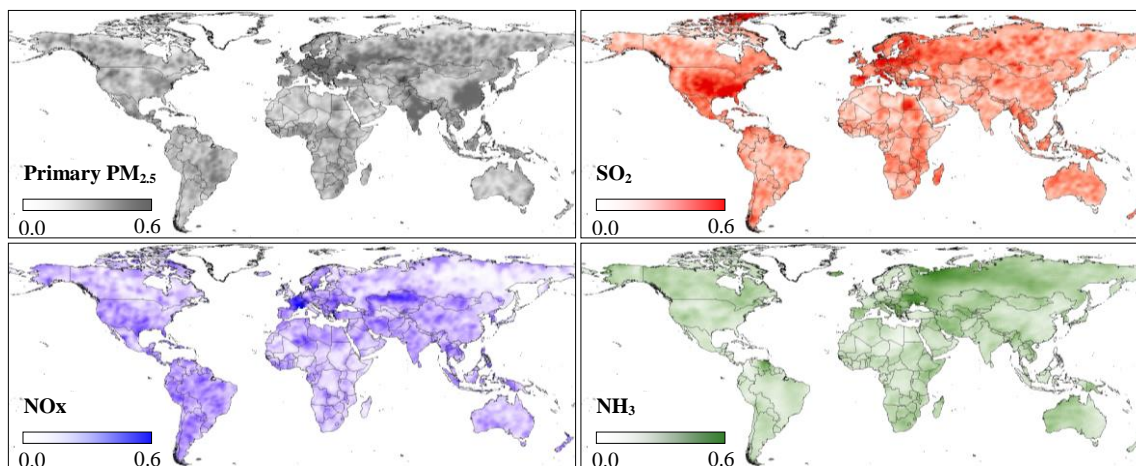


**Fig. 2** Geospatial distribution of partial correlation coefficients between the emissions of major air pollutants and  $PM_{2.5}$  concentrations. The four pollutants are primary  $PM_{2.5}$ ,  $SO_2$ ,  $NO_x$ , and  $NH_3$ .

183 Similarly, significant partial correlations ( $p < 0.05$ ) were found between the main meteorological  
 184 parameters and  $PM_{2.5}$  concentrations derived from the fixed-emission scenario simulation. On average, the  
 185 most important parameter is air temperature (T), with a correlation of 0.22 followed by wind speed (WS,  $r$   
 186 = -0.16), planetary boundary layer height (PBLH,  $r = -0.16$ ), relative humidity (RH,  $r = 0.14$ ), and surface  
 187 pressure (SP,  $r = -0.14$ ). These results correspond with those of a previous study<sup>7,14,37</sup> The geospatial  
 188 distribution of the main meteorological parameters is shown in **Fig. S6**. In cold, high-latitude regions of  
 189 North America and Siberia and in warm regions extending from northern Africa to the Arabian Peninsula,  
 190  $PM_{2.5}$  concentrations are mostly sensitive to temperature, which is partially associated with  
 191 temperature-sensitive  $SO_2$ <sup>38</sup>. The effects of WS or PBLH are stronger in regions with relatively high  
 192 elevations, where strong winds facilitate dispersion<sup>7,14,37</sup>, whereas the presence of low PBLH levels predict  
 193 a stable atmosphere<sup>39</sup>. WS and PBLH are also important in many other regions, including Southeast Asia,  
 194 Brazil, and the eastern seaboard of Australia, where tropical or subtropical monsoons prevail<sup>40</sup>. In dry  
 195 inland regions such as central Eurasia, the formation of secondary  $PM_{2.5}$  is more sensitive to RH<sup>41</sup>. To  
 196 characterize the relationship between emissions and meteorological effects, the relative contributions of

197 emissions ( $RC_E$ ) and meteorological conditions ( $RC_M$ ) were measured across all model gridcells based on  
198 the results of the three conditional scenario simulations. The mean daily/weekly  $RC_M$  values for  $PM_{2.5}$   
199 ( $68\% \pm 5\%/63\% \pm 5\%$ ) are much higher than the mean daily/weekly  $RC_E$  values for  $PM_{2.5}$   
200 ( $32\% \pm 5\%/37\% \pm 5\%$ ) ( $p < 0.05$ ). Emissions become more significant on a seasonal/annual basis. For  
201 example, mean seasonal  $RC_E$  is  $54\% \pm 7\%$ . Changes in emissions on these longer time scales are largely  
202 driven by seasonal emission cycles<sup>23,42</sup> and by long-term socioeconomic patterns<sup>43</sup>.

203 In addition to annual mean  $PM_{2.5}$  concentrations, the number of severely polluted days (NSPD, defined as  
204 the number of days with daily  $PM_{2.5}$  values of  $> 150 \mu\text{g}/\text{m}^3$ ) is of particular interest not only because the  
205 annual mean concentrations are significantly associated with these high values<sup>44</sup> but also because public  
206 responses to extreme conditions are stronger<sup>45</sup>. The occurrence of heavy pollution episodes is often  
207 associated with stable meteorological conditions, as emissions do not usually change dramatically on a  
208 daily basis<sup>46</sup>. **Fig. S7a** compares temporal variations of the NSPD for Beijing (from the realistic-case  
209 simulation) to emissions of major air pollutants for the surrounding area (Beijing-Tianjin-Hebei) for the  
210 winter months from 2000 to 2014. Although the NSPD and emissions undergo similar increasing trends,  
211 they are not always synchronous on an annual basis due to the influence of meteorological conditions. For  
212 example, a sharp increase in the NSPD observed from 2012 to 2013 was not driven by emission increases  
213 but by unusual meteorological conditions<sup>46,47</sup>. During that winter, the seasonal averaged WS dropped from  
214 a long-term mean of 2.94 to 2.33 m/s, and the number of days of abnormally high humidity ( $RH > 75\%$ )  
215 and extremely low PBLH ( $< 150 \text{ m}$ ) increased from 3% to 10% and from 6.3% to 8.4%, respectively (**Fig.**  
216 **S7b-f**), favoring the growth of secondary aerosols and the accumulation of air pollutants at the ground  
217 level<sup>48,49</sup>.

218 **Emission-based Prediction.** As discussed above, annual mean  $PM_{2.5}$  concentrations for the 35-year period  
219 derived from the fixed-meteorology simulation are significantly correlated with emissions observed across  
220 individual model gridcells. Such a correlation suggests that a set of regression models can be developed to  
221 predict  $PM_{2.5}$  concentrations based on emissions with meteorological confounding effects excluded. If such  
222 models can be validated against the output of the fixed-meteorology simulation, they can be applied to  
223 simulate historical  $PM_{2.5}$  trends-based exclusively on emissions and to predict emission-driven future  $PM_{2.5}$   
224 trends. As confounding meteorological effects are eliminated by these models, the proposed method

225 enables us to evaluate the effectiveness of emission-reduction efforts. To do so, the emissions of the four  
226 most important air pollutants identified based on a sensitivity analysis, primary PM<sub>2.5</sub>, SO<sub>2</sub>, NH<sub>3</sub>, and NO<sub>x</sub>,  
227 were used as independent variables in developing multivariate regression models, whereas PM<sub>2.5</sub>  
228 concentrations derived from the fix-meteorology simulation were used as a dependent variable. As both  
229 emission densities and PM<sub>2.5</sub> concentrations are log-normally distributed (**Fig. S8**), the multivariate  
230 regression models were fitted to all model gridcells using log-transformed data and were applied to  
231 calculate annual mean PM<sub>2.5</sub> concentrations for these gridcells. As the formation of secondary aerosols in  
232 the air does not linearly respond to precursor emissions<sup>3</sup>, several nonlinear equations were tested with no  
233 significant improvements observed in the results. Given that the statistical regression models were  
234 established to predict annual PM<sub>2.5</sub>, the nonlinearity of the secondary aerosol formation, which occurred in  
235 a short time ranging from seconds to diurnal, was filtered out by the annual means. As such, the following  
236 linear model was adopted.

$$237 \log PM_{2.5} = \sum a_i \log E_i + b,$$

238 where  $PM_{2.5}$  is annual mean PM<sub>2.5</sub> concentration,  $E_i$  are annual emissions of the  $i^{\text{th}}$  pollutants,  $a_i$  and  $b$  are  
239 regression coefficients. **Fig. S9** shows the spatial distribution of  $R^2$  values of the regression models,  
240 indicating that results for areas characterized by high emission levels and population densities are much  
241 better ( $R^2$  values are close to one) than those found for other regions, which is helpful in reducing overall  
242 uncertainty. The regression models were validated by plotting the predicted PM<sub>2.5</sub> concentrations against  
243 those derived from the fixed-meteorology scenario simulation shown in **Fig. S10** for China, India, the  
244 United States, and Germany. This good agreement suggests that the models could be used to predict annual  
245 PM<sub>2.5</sub> concentrations with reasonable accuracy, while confounding meteorological effects were not taken  
246 into account. It should be pointed out that the potential impact of climate change was not taken into  
247 consideration.

248 The simplified approach to predicting annual mean ambient PM<sub>2.5</sub> concentrations at the ground level based  
249 on annual total emissions omits the exchanges occurring among gridcells due to transport. Although the  
250 association between the emissions and PM<sub>2.5</sub> concentrations at a given gridcell can be disturbed by the  
251 atmospheric transport across gridcells, the influence of the atmospheric transport on the association is  
252 weakened by similarities among adjacent model gridcells. Such similarities were demonstrated by the spatial

253 autocorrelation of the regression model parameters. On a global scale, the calculated Moran's  
254 autocorrelation indexes are valued at 0.39 (intercepts), 0.50 (slopes for primary  $PM_{2.5}$ ), 0.33 (slopes for  
255  $SO_2$ ), 0.36(slopes for  $NO_x$ ), and 0.30 (slopes for  $NH_3$ ) and are statistically significant ( $p < 0.05$ ). As was  
256 expected, such autocorrelation is also significant for the gridded emissions and  $PM_{2.5}$  concentrations and  
257 Moran's autocorrelation indexes vary from 0.25 to 0.52 for gridded emissions of the four pollutants and are  
258 as high as 0.75 for gridded  $PM_{2.5}$  concentrations ( $p < 0.05$ ). The most significant autocorrelation of  $PM_{2.5}$   
259 concentrations is attributed to the dispersion of  $PM_{2.5}$  in the air. Due to the autocorrelation of emissions,  
260 emissions observed at individual gridcells also shape emissions from the surrounding gridcells.

261 **Meteorology-related Variations.** As discussed above, interannual trends of emission-driven  $PM_{2.5}$   
262 concentrations excluding meteorological confounding effects can be predicted based on annual emissions  
263 from data generated from the fixed-meteorology simulation. Similarly, the outputs of the fixed-emission  
264 simulation provide the information on variations in  $PM_{2.5}$  concentrations caused by confounding  
265 meteorological effects. As the influence of meteorological factors randomly fluctuates based on  
266 emission-induced  $PM_{2.5}$  concentrations, the following probabilistic function was used to characterize such  
267 random effects:

$$268 \quad F(PM_{2.5}) = (2\pi\sigma)^{-0.5}\exp(-PM_{2.5}^2/2\sigma^2),$$

269 where  $F(PM_{2.5})$  is a probability function,  $PM_{2.5}$  is annual mean  $PM_{2.5}$  concentration, and  $\sigma$  is standard  
270 deviation associated with change in meteorological conditions under the fixed emission. Based on annual  
271 mean  $PM_{2.5}$  concentrations calculated from the fixed-emission simulation for the 35 years spanning from  
272 1980 to 2014, probabilistic functions were derived for all individual gridcells on an annual scale. For most  
273 of the gridcells (84%) the functions are normally distributed ( $p > 0.05$ ). Deviations from the normal  
274 distribution are mostly observed in deserts or surrounding areas (**Fig. S11**). For the fixed-meteorology  
275 simulation the year 2014 is assumed to be a "normal" year for which most meteorological parameters are  
276 approximately equal to the 35-year mean with a standardized deviation of  $0.12\pm 0.25$ . This assumption is  
277 confirmed by calculating the average deviation of annual  $PM_{2.5}$  concentrations derived from 2014  
278 meteorology trends to average values for 1980 to 2014 based on the fixed-emission simulation. It was  
279 found that relative deviations for 95% of all model gridcells are less than 5%, and the overall mean value of  
280 deviation for all gridcells is  $0.072\%\pm 1.1\%$  (mean and standard deviation), which is not significantly

281 different from zero ( $p < 0.05$ ) as was expected. Therefore, the frequency distribution generated from the  
282 fixed-emission simulation represents random variations resulting from confounding meteorological effects.  
283 The robustness of the function was also tested using a Jackknife test for a randomly selected gridcell. The  
284 test was conducted 35 times by removing calculated 35  $PM_{2.5}$  concentrations from the fixed-emission  
285 simulation one by one and by generating probabilistic distributions based on the 34 remaining datasets. The  
286 mean and standard deviation of the 35 repeated calculations are  $3 \times 10^{-17} \pm 5 \times 10^{-17}$  and  $0.04 \pm 0.001$ ,  
287 respectively, indicating a very high degree of robustness.

288 In fact, the probabilistic functions can be derived either on an annual basis or on any temporal scale from a  
289 daily to seasonal basis. **Fig. 3** shows typical examples of the probabilistic functions for a typical gridcell  
290 (Guangzhou, China) on annual (a), monthly (b), and daily (c) scales. The majority of these functions reflect  
291 typical normal distributions, which is more evident on a shorter time scale. On an annual scale, the annual  
292 mean  $PM_{2.5}$  concentration changes considerably with a coefficient of variation (CV) of 14%. Even without  
293 any change in emissions, the annual mean  $PM_{2.5}$  concentration presents a 48% chance of increasing or may  
294 decrease by more than 10%. This means that while emission-mitigation measures can reduce ambient  $PM_{2.5}$   
295 concentrations by 10% in a single year for this gridcell, there is a more than 20% chance of the observed  
296 annual mean concentration not declining at all or even of increasing. Similarly, the likelihood of the annual  
297 mean decreasing by more than 20% is also higher than 20%. Therefore, simply comparing annual mean  
298  $PM_{2.5}$  concentrations of two consecutive years without taking meteorological conditions into consideration  
299 can be misleading. Upon reducing the time scale from annual to monthly and daily, the variation in  
300 probabilistic functions increases. CV values for monthly and daily  $PM_{2.5}$  concentrations increase to 29%  
301 and 38%, respectively, for the selected gridcell, which are significantly higher values than those found for  
302 annual data and which can be explained by the fact that daily and monthly meteorological conditions vary  
303 more dramatically than emissions. Therefore, monthly meteorological factor-forced changes are more  
304 random than those observed on an annual scale. With constant emissions there is a more than 50%  
305 probability of a 20% change occurring in monthly mean  $PM_{2.5}$  concentrations. Therefore, it is even riskier  
306 to directly compare mean  $PM_{2.5}$  concentrations of a given month to those for the same period of a previous  
307 year while disregarding random confounding meteorological effects.

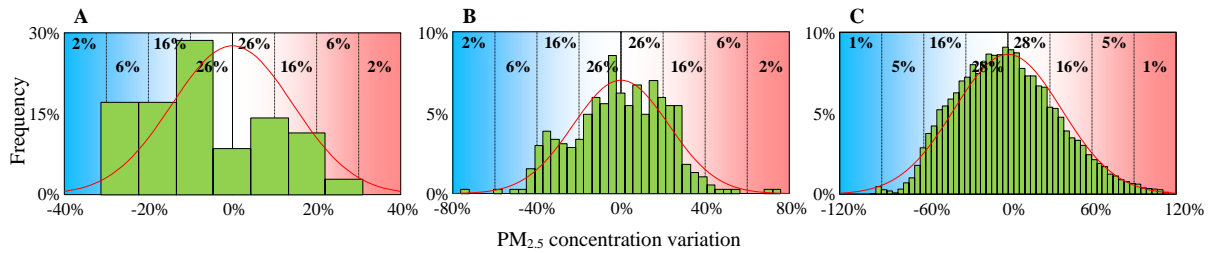


**Fig. 3** Probabilistic functions derived from fixed-emission simulations of annual (A), monthly (B), and daily resolutions (C) for a representative gridcell. Bars denote the frequency distribution of the model-calculated PM<sub>2.5</sub> concentrations normalized by corresponding mean values with a fitted normal distribution curve. The probabilities of individual segments are shown in the background.

308 The random variation observed in the calculated probabilistic function is a direct indicator of the extent of  
 309 confounding meteorological effects on individual gridcells. To quantify overall variations on a global scale,  
 310 annual mean-based CVs were calculated for all gridcells. Corresponding results are shown in **Fig. S12** as a  
 311 cumulative distribution of CVs for all gridcells. The mean and standard deviation of the CV values are  
 312  $16 \pm 11\%$  (median is 14.2%) with a maximum value of 109%. On average, confounding meteorological  
 313 factors can lead to more than one-sixth of a variation at 28% for all model gridcells. The contribution can  
 314 be as high as 100% in extreme cases. As discussed above, short-term variations observed over less than one  
 315 year are even larger. When monthly data are used, the mean and standard deviation of the CV values are  
 316  $65 \pm 35\%$ , showing stronger seasonal variations. The maximum CV of an individual gridcell can reach 200%  
 317 on a monthly scale. Again, significant autocorrelations (Moran's index = 0.59,  $p < 0.05$ ) were found for the  
 318 probabilistic functions (CVs) on an annual scale, denoting continuity in meteorological effects across  
 319 space.

320 The annual change in confounding meteorological effects on globally averaged PM<sub>2.5</sub> concentrations,  
 321 defined as a normalized global average PM<sub>2.5</sub> anomaly for individual year from the 35-year mean, was  
 322 calculated from 1980 to 2014 based on the fixed-emission simulation. The deviations observed reflect the  
 323 average influence of annual meteorological conditions on annual mean PM<sub>2.5</sub> concentrations on a global  
 324 scale. It should be noted that the annual deviation observed in 2014 was the smallest, showing that using  
 325 meteorological parameters for 2014 as a "normal" year for our fixed-meteorological simulations is the best  
 326 choice for the 35 years studied. Such annual changes are often affected by global atmospheric circulation<sup>50</sup>.  
 327 It is interesting to observe that the interannual anomalies of meteorological effects are significantly  
 328 correlated with Arctic Oscillation (AO), which is shown as solid dots in **Fig. 4** ( $r = 0.66$ ,  $p < 0.05$ ). Some  
 329 regional studies also show a similar relationship. For example, it was reported that enhanced dust emissions



330 observed across Saharan regions and the increasing frequency of haze episodes recorded in northern China  
331 are associated with the positive phase of AO<sup>10,51</sup>.

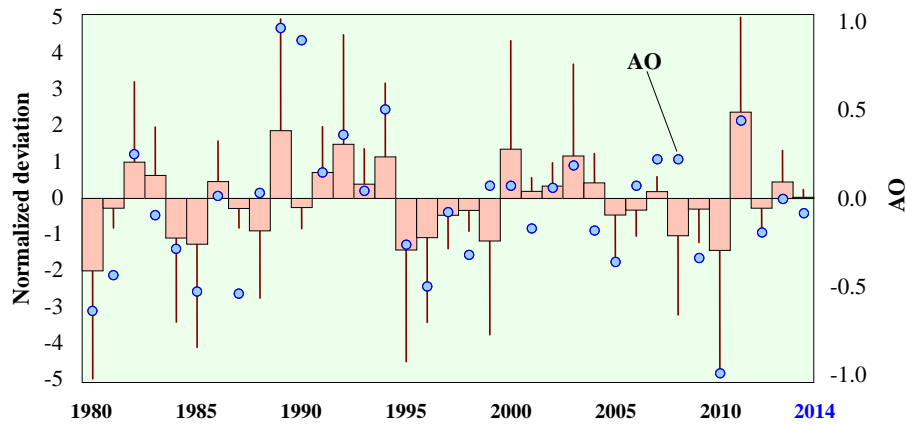


**Fig. 4** Normalized global average deviation of PM<sub>2.5</sub> concentrations from the mean value for the 35 years spanning from 1980 to 2014 (bars). The results are based on a fixed-emission simulation conducted at the global scale. Standard deviations are shown as dark red lines. The blue dots denote Arctic Oscillation.

332 To further illustrate spatial variations in meteorological-induced variation,  $UI_{95}$  values are mapped in **Fig.**  
333 **S13** in both absolute and relative terms. The global average  $UI_{95}$  of annual PM<sub>2.5</sub> concentrations was  
334 measured as 4.9  $\mu\text{g}/\text{m}^3$  (40%). Hot regions of absolute variation exhibit strong meteorological variations. In  
335 addition to areas around deserts (e.g., the southern Sahara and the Middle East) where dust forms a major  
336 component of PM<sub>2.5</sub> emissions and where concentrations are subject to synoptic-scale weather patterns<sup>51</sup>,  
337 strong variations in PM<sub>2.5</sub> concentrations can be observed in heavily polluted regions such as the North  
338 China Plain (NCP) and likely due to interactions between high emissions and highly variable  
339 meteorological patterns<sup>9,46</sup>. On the other hand, relatively large values of relative terms are often observed in  
340 regions with low levels of population density and low PM<sub>2.5</sub> concentrations. For example, very high levels  
341 of relative variability were found in high-latitude regions and coastal areas, where background PM<sub>2.5</sub>  
342 concentrations are very low. In most high-emission regions (e.g., eastern China, India, Europe, the United  
343 States), although PM<sub>2.5</sub> variations induced by meteorological conditions are lower, high PM<sub>2.5</sub> levels can  
344 increase absolute variations on a considerable scale. For example, the  $UI_{95}$  for northern India and for the  
345 NCP are as high as 11.5  $\mu\text{g}/\text{m}^3$  and 20.6  $\mu\text{g}/\text{m}^3$ , respectively.

346 **Model Application.** When the regression model predictions and probabilistic functions are combined,  
347 annual mean PM<sub>2.5</sub> concentration trends driven by emissions coupled with meteorological effects can be  
348 quantified. The concentration predicted by the regression model provides an estimation of the annual mean

349 PM<sub>2.5</sub> under given emissions and average meteorological conditions, whereas a range derived from the  
350 probabilistic function at a fixed probability (e.g., 95%) shows fluctuation associated with random variations  
351 of meteorological parameters. This approach was then applied to simulate global historical temporal trends  
352 of PM<sub>2.5</sub> concentrations from 1980 to 2014 and to project future trends from 2015 to 2030. Emission-driven  
353 trends of global annual mean PM<sub>2.5</sub> concentrations prior to 2015 were calculated from the gridcell  
354 regression models based on PKU series emission inventories<sup>19</sup> and from the RCP (Representative  
355 Concentration Pathways)2.6 and RCP8.5 emission scenarios model run for after 2014<sup>52,53</sup> using emissions  
356 for 2014 as a baseline. The results are denoted by the solid line shown in **Fig. S14a**. In the figure,  
357 meteorological condition-induced variation ranges are shown by the darkly shaded *UI*<sub>50</sub> and lightly shaded  
358 *UI*<sub>95</sub>. We further assume that meteorological conditions for 2014 used as a "normal" year can be extended  
359 to future years. For the past 35 years, global annual mean PM<sub>2.5</sub> concentrations decreased slightly from 13.1  
360 µg/m<sup>3</sup> (10.4~16.1 µg/m<sup>3</sup> as *UI*<sub>50</sub>) to 12.1 µg/m<sup>3</sup> (9.8~14.6 µg/m<sup>3</sup>), and decreasing trends tend to continue in  
361 the future at a slightly faster rate, which could be attributed to increasing awareness and to  
362 emission-mitigation efforts made by many developing countries, especially China. We found slight  
363 differences in projected PM<sub>2.5</sub> levels between the two emission scenarios on a global scale prior to 2030. It  
364 should be noted that the probability functions were developed based on gridded meteorological parameters.  
365 When the results are presented on an area with more than one gridcell, such as a country, a city, or even the  
366 globe, the calculated *UI* values are simply averaged over gridcells covering the area. This practice is based  
367 on the assumption that all meteorological confounding factors do not vary significantly within the region of  
368 concern. This applies to a relatively small region such as the NCP, where a somewhat uniform surface  
369 pressure with small pressure gradients is often observed, which in turn produces fewer altered wind and  
370 temperature fields across the NCP. However, for a larger region such as China or a region with complex  
371 terrain, this assumption would lead to an overestimation of *UI* values. Unfortunately, the accuracy of the *UI*  
372 estimation is difficult to enhance, as spatial similarities in changes of meteorological parameters are  
373 difficult to quantify. To further validate the model-calculated PM<sub>2.5</sub> concentrations using the regression  
374 models, the calculated PM<sub>2.5</sub> concentrations for before 2014 are compared to those observed from various  
375 monitoring stations (gridcells) over various years in **Fig. S14b-c**. Both calculated annual mean  
376 concentrations (dots) and *UI* values (bars, b. *UI*<sub>50</sub> and c. *UI*<sub>95</sub>) are shown, indicating a good agreement.  
377 The method was further applied to various countries to predict annual mean PM<sub>2.5</sub> concentrations subject to

378 the changes in emissions. Corresponding results are shown in **Fig. 5** for 12 countries. The projected  $PM_{2.5}$   
379 trend for 1980 to 2030 from the regression model was obtained based on RCP2.6 and RCP8.5 emission  
380 scenarios<sup>52,53</sup>. In general, these trends and *UI* values vary significantly across countries. Relatively high  
381 levels of variability observed for some countries are associated with stronger changes in meteorological  
382 conditions and especially for monsoon regions (e.g., China and Pakistan) where the strength of prevailing  
383 monsoons play an important role in aerosol production and dispersion<sup>10,54</sup>. The results also show that for  
384 developed countries such as the United States, France, and Japan, past declines in  $PM_{2.5}$  will remain with  
385 slight differences between RCP2.6 and RCP8.5 predictions. Trends for France are an exception, as the  
386 RCP2.6 assumes a much stronger decrease in pollutant emissions and hence in  $PM_{2.5}$  concentrations.  
387 Predicted  $PM_{2.5}$  concentration trends vary substantially across developing countries. In China, annual mean  
388  $PM_{2.5}$  concentrations tend to decrease continuously, which is consistent with considerable efforts made to  
389 curb air pollution in recent years<sup>16</sup>. For other developing countries such as India and Indonesia,  $PM_{2.5}$   
390 concentrations are projected to increase continuously until 2020 if the proposed emission scenarios are not  
391 altered. As the RCPs dataset provides emission data at a decadal temporal resolution, tipping points from  
392 emission incline to decline cannot be precisely identified. Nevertheless, these trends imply that although  
393 severe levels of air pollution have spurred widespread awareness and concern from governments and the  
394 public, efficient mitigation is still lacking in most developing countries. Meanwhile, it is very likely that air  
395  $PM_{2.5}$  concentrations will increase continuously in coming years in developing countries such as Laos and  
396 in Central Africa.

397 **Fig. S15** shows three examples of predicted historical and future trends of  $PM_{2.5}$  concentrations for three  
398 cities for which recent monitoring data are available, based on the RCP2.6 and RCP8.5 emission  
399 scenarios<sup>52,53</sup> for 1980 to 2030. For the city of New York,  $PM_{2.5}$  monitoring data for after 2014 suggest that  
400 emission-reduction rates likely range between the two scenarios, which are not remarkably different in the  
401 first place. For New Delhi, although the observed values still fall within the  $UI_{95}$  range, concentrations  
402 reported for the last three years exceed the predicted means. Although unusual meteorological conditions  
403 could play a critical role in increasing concentrations, relatively high levels of  $PM_{2.5}$  observed for 2014 and  
404 2016 may indicate accelerated increases in emission and pollution levels. Numerous studies have reported  
405 high levels of air pollution in India in recent years<sup>55</sup>. Beijing is one of the most heavily contaminated cities  
406 in northern China. Based on both RCP2.6 and RCP8.5 emission scenarios, we find a slight decline in  $PM_{2.5}$

407 concentrations after 2014. However, the measured annual mean  $PM_{2.5}$  concentrations from 2014 to 2016  
 408 are well below the predicted ones and even fall below the lower bound of the 95% uncertainty interval. It is  
 409 likely that mitigation measures applied in the city were more effective than what was planned in RCP  
 410 scenarios.

411 In summary, the novel method developed in this study serves as a useful tool for quantifying  
 412 emission-induced changes in  $PM_{2.5}$  concentrations by excluding confounding meteorological effects. The  
 413 approach involves less computation than an atmospheric chemical transport model; hence it can be used in  
 414 quantitative environments, for health assessments of  $PM_{2.5}$  and to evaluate the effectiveness of mitigation  
 415 efforts. Importantly, we learned from this study that long-term trends rather than declines occurring over a  
 416 single year are critical to consider when evaluating the effectiveness of mitigation measures while  
 417 considering meteorology-induced  $PM_{2.5}$  fluctuations.

418

419

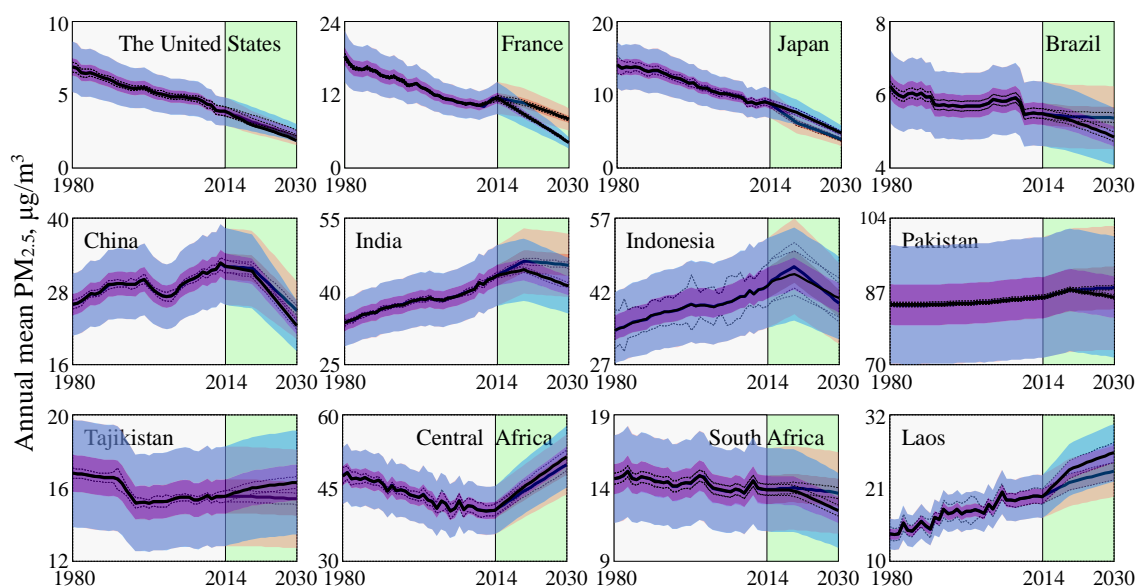


**Fig. 5** Temporal trends of  $PM_{2.5}$  concentrations for 12 countries for 1980 to 2030 based on the RCP2.6 (blue) and RCP8.5 (orange) emission scenarios. Emission-driven trends are shown as medians (black lines) with a 90% confidence interval (black dash lines). Potential fluctuations induced by meteorological confounding effects are shown as shaded areas as  $UI_{50}$  (dark shaded area) and  $UI_{95}$  (light shaded area).

420 **AUTHOR INFORMATION**

421 **Corresponding Author**

422 \*Phone and Fax: +86-10-62751938. E-mail: taos@pku.edu.cn

423

424 **Notes**

425 The authors declare no competing financial interests.

426 **ACKNOWLEDGMENTS**

427 This work was funded by the National Natural Science Foundation of China (Grant 41571130010,  
428 41390240, and 41629101), the 111 program (B14001), and the Undergraduate Student Research  
429 Training Program.

430 **ASSOCIATED CONTENT**

431 Supporting Information. Detailed results of the sensitivity analysis for key pollutants, various model  
432 validations, spatial distributions of major meteorological parameters, comparisons drawn between  
433 emissions and PM<sub>2.5</sub> concentrations, frequency distributions of emissions and PM<sub>2.5</sub> concentrations,  
434 spatial distributions of regression model  $R^2$  values, meteorological effect-induced variations,  
435 cumulative distributions of CVs, and predicted trends for 3 cities are freely available at  
436 <http://pubs.acs.org>.

437

438

439 **References**

- 440 (1) Lelieveld, J.; Evans, J. S.; Fnais, M.; Giannadaki, D.; Pozzer, A. The contribution of outdoor air pollution sources to  
441 premature mortality on a global scale. *Nature* **2015**, *525* (7569), 367-371.
- 442 (2) Cohen, A. J.; Brauer, M.; Burnett, R.; Anderson, H. R.; Frostad, J.; Estep, K.; Balakrishnan, K.; Brunekreef, B.;  
443 Dandona, L.; Dandona, R.; Feigin, V.; Freedman, G.; Hubbell, B.; Jobling, A.; Kan, H.; Knibbs, L.; Liu, Y.; Martin, R.;  
444 Morawska, L.; Pope III, C. A.; Shin, H.; Straif, K.; Shaddick, G.; Thomas, M.; van Dingenen, R.; van Donkelaar, A.;  
445 Vos, T.; Murray, C. J. L.; Forouzanfar, M. H. Estimates and 25-year trends of the global burden of disease attributable  
446 to ambient air pollution: an analysis of data from the Global Burden of Diseases Study 2015. *Lancet* **2017**, *389* (10082),  
447 1907-1918.
- 448 (3) Ansari, A. S.; Pandis, S. N. Response of Inorganic PM to Precursor Concentrations. *Environ. Sci. Technol.* **1998**, *32*,  
449 2706-2714.
- 450 (4) Hueglin, C.; Gehrig, R.; Baltensperger, U.; Gysel, M.; Monn, C.; Vonmont, H. Chemical characterisation of PM<sub>2.5</sub>,  
451 PM<sub>10</sub> and coarse particles at urban, near-city and rural sites in Switzerland. *Atmos. Environ.* **2005**, *39* (4), 637-651.
- 452 (5) Liu, J.; Mauzerall, D. L.; Chen, Q.; Zhang, Q.; Song, Y.; Peng, W.; Klimont, Z.; Qiu, X.; Zhang, S.; Hu, M.; Lin, W.;  
453 Smith, K. R.; Zhu, T. Air pollutant emissions from Chinese households: A major and underappreciated ambient  
454 pollution source. *Proc. Natl. Acad. Sci. USA* **2016**, *113* (28), 7756-7761.
- 455 (6) Zhang, H.; Hu, D.; Chen, J.; Ye, X.; Wang, S. X.; Hao, J. M.; Wang, L.; Zhang, R.; An, Z. Particle size distribution and  
456 polycyclic aromatic hydrocarbons emissions from agricultural crop residue burning. *Environ. Sci. Technol.* **2011**, *45*  
457 (13), 5477-5482.
- 458 (7) Tai, A. P. K.; Mickley, L. J.; Jacob, D. J. Correlations between fine particulate matter (PM<sub>2.5</sub>) and meteorological  
459 variables in the United States: Implications for the sensitivity of PM<sub>2.5</sub> to climate change. *Atmos. Environ.* **2010**, *44* (32),  
460 3976-3984.
- 461 (8) DeGaetano, A. Temporal, spatial and meteorological variations in hourly PM<sub>2.5</sub> concentration extremes in New York  
462 City. *Atmos. Environ.* **2004**, *38* (11), 1547-1558.
- 463 (9) Sun, Y.; Chen, C.; Zhang, Y.; Xu, W.; Zhou, L.; Cheng, X.; Zheng, H.; Ji, D.; Li, J.; Tang, X.; Fu, P.; Wang, Z. Rapid  
464 formation and evolution of an extreme haze episode in Northern China during winter 2015. *Sci. Rep.* **2016**, *6*, 27151.
- 465 (10) Zou, Y.; Wang, Y.; Zhang, Y.; Koo, J. H. Arctic sea ice, Eurasia snow, and extreme winter haze in China. *Sci. Adv.* **2017**,  
466 *3* (3), e1602751.
- 467 (11) Guo, S.; Hu, M.; Zamora, M. L.; Peng, J.; Shang, D.; Zheng, J.; Du, Z.; Wu, Z.; Shao, M.; Zeng, L.; Molina, M. J.;  
468 Zhang, R. Elucidating severe urban haze formation in China. *Proc. Natl. Acad. Sci. USA* **2014**, *111* (49), 17373-17378.
- 469 (12) Wang, Y.; Yao, L.; Wang, L.; Liu, Z.; Ji, D.; Tang, G.; Zhang, J.; Sun, Y.; Hu, B.; Xin, J. Mechanism for the formation of  
470 the January 2013 heavy haze pollution episode over central and eastern China. *Sci. China Earth Sci.* **2013**, *57* (1),  
471 14-25.
- 472 (13) Zhao, X. J.; Zhao, P. S.; Xu, J.; Meng, W.; Pu, W. W.; Dong, F.; He, D.; Shi, Q. F. Analysis of a winter regional haze  
473 event and its formation mechanism in the North China Plain. *Atmos. Chem. Phys.* **2013**, *13* (11), 5685-5696.
- 474 (14) Shen, L.; Mickley L. J.; Murray, L. T. Influence of 2000-2050 climate change on particulate matter in the United States:  
475 results from a new statistical model. *Atmos. Chem. Phys.* **2017**, *17*, 4355-4367.
- 476 (15) Ministry of Environmental Protection of the People's Republic of China (MEP),  
477 [http://www.zhb.gov.cn/gkml/hbb/qt/201707/t20170725\\_418538.htm](http://www.zhb.gov.cn/gkml/hbb/qt/201707/t20170725_418538.htm) (accessed 2017.12).
- 478 (16) Qin, Y.; Wagner, F.; Scovronick, N.; Peng, W.; Yang, J.; Zhu, T.; Smith, K. R.; Mauzerall, D. L. Air quality, health, and  
479 climate implications of China's synthetic natural gas development. *Proc. Natl. Acad. Sci. USA* **2017**, *114* (19),  
480 4887-4892.
- 481 (17) Liu, Y.; Wu, Z.; Wang, Y.; Xiao, Y.; Gu, F.; Zheng, J.; Tan, T.; Shang, D.; Wu, Y.; Zeng, L.; Hu, M.; Bateman, A. P.;  
482 Martin, S. T. Submicrometer Particles Are in the Liquid State during Heavy Haze Episodes in the Urban Atmosphere of

- 483 Beijing, China. *Environ. Sci. Tech. Let.* **2017**, *4* (10), 427-432.
- 484 (18) Emmons, L. K.; Walters, S.; Hess, P. G.; Lamarque, J. F.; Pfister, G. G.; Fillmore, D.; Granier, C.; Guenther, A.;  
485 Kinnison, D.; Laepple, T.; Orlando, J.; Tie, X.; Tyndall, G.; Wiedinmyer, C.; Baughcum, S. L.; Kloster, S. Description  
486 and evaluation of the Model for Ozone and Related chemical Tracers, version 4 (MOZART-4). *Geosci. Model Dev.*  
487 **2010**, *3*, 43-67.
- 488 (19) Peking University Inventory Dataset, version 2. <http://inventory.pku.edu.cn/> (accessed 2017.7).
- 489 (20) Crippa, M.; Guizzardi, D.; Muntean, M.; Schaaf, E.; Dentener, F.; van Aardenne, J. A.; Monni, S.; Doering, U.; Olivier,  
490 J. G. J.; Pagliari, V.; Janssens-Maenhout, G. Gridded Emissions of Air Pollutants for the period 1970–2012 within  
491 EDGAR v4.3.2. *Earth Syst. Sci. Data Discuss.* **2018**, DOI.org/10.5194/essd-2018-31
- 492 (21) Janssens-Maenhout, G.; Crippa, M.; Guizzardi, D.; Dentener, F.; Muntean, M.; Pouliot, G.; Keating, T.; Zhang, Q.;  
493 Kurokawa, J.; Wankmüller, R.; van der Gon, H. D.; Kuenen, J. J. P.; Klimont, Z.; Frost, G.; Darras, S.; Koffi, B.; Li, M.  
494 HTAP\_v2.2: a mosaic of regional and global emission grid maps for 2008 and 2010 to study hemispheric transport of  
495 air pollution. *Atmos. Chem. Phys.* **2015**, *15*, 11411-11432.
- 496 (22) Sindelarova, K.; Granier, C.; Bouarar, I.; Guenther, A.; Tilmes, S.; Stavrou, T.; Müller, J. F.; Kuhn, U.; Stefani, P.;  
497 Knorr, W. Global data set of biogenic VOC emissions calculated by the MEGAN model over the last 30 years. *Atmos.*  
498 *Chem. Phys.* **2014**, *14* (17), 9317-9341.
- 499 (23) van der Werf, G. R.; Randerson, J. T.; Giglio, L.; van Leeuwen, T. T.; Chen, Y.; Rogers, B. M.; Mu, M.; van Marle, M. J.  
500 E.; Morton, D. C.; Collatz, G. J.; Yokelson, R. J.; Kasibhatla, P. S. Global fire emissions estimates during 1997-2016.  
501 *Earth Syst. Sci. Data* **2017**, *9* (2), 697-720.
- 502 (24) Kalnay, E.; Kanamitsu, M.; Kistler, R.; Collins, W.; Deaven, D.; Gandin, L.; Iredell, M.; Saha, S.; White, G.; Woollen, J.;  
503 Zhu, Y.; Chelliah, M.; Ebisuzaki, W.; Higgins, W.; Janowiak, J.; Mo, K. C.; Ropelewski, C.; Wang, J.; Leetmaa, A.;  
504 Reynolds, R.; Jenne, R.; Joseph, D. The NCEP/NCAR 40-Year Reanalysis Project. *B. Am. Meteorol. Soc.* **1996**, *77*,  
505 437-471.
- 506 (25) Levy, R. C.; Remer, L. A.; Kleidman, R. G.; Mattoo, S.; Ichoku, C.; Kahn, R.; Eck, T. F. Global evaluation of the  
507 Collection 5 MODIS dark-target aerosol products over land. *Atmos. Chem. Phys.* **2010**, *10* (21), 10399-10420.
- 508 (26) van Donkelaar, A.; Martin, R. V.; Brauer, M.; Kahn, R.; Levy, R.; Verduzco, C.; Villeneuve, P. J. Global estimates of  
509 ambient fine particulate matter concentrations from satellite-based aerosol optical depth: development and application.  
510 *Environ. Health Perspect.* **2010**, *118* (6), 847-855.
- 511 (27) IBM SPSS Statistics Manuals. <https://www-01.ibm.com/support/docview.wss?uid=swg27038407#en> (accessed 2015).
- 512 (28) MathWorks Documentation for MATLAB. [https://www.mathworks.com/help/pdf\\_doc/matlab/index.html](https://www.mathworks.com/help/pdf_doc/matlab/index.html)(accessed  
513 2016.12).
- 514 (29) Mahmud, A.; Barsanti, K., Improving the representation of secondary organic aerosol (SOA) in the MOZART-4 global  
515 chemical transport model. *Geosci. Model Dev.* **2013**, *6*, 961–980.
- 516 (30) Valorso, R., Aumont, B., Camredon, M., Raventos-Duran, T., Mouchel-Vallon, C., Ng, N. L., Seinfeld, J. H., Lee-Taylor,  
517 J., and Madronich, S.: Explicit modelling of SOA formation from  $\alpha$ -pinene photooxidation: sensitivity to vapour  
518 pressure estimation. *Atmos. Chem. Phys.* **2011**, *11*, 6895-6910.
- 519 (31) Zhang, L.; Liu, L.; Zhao, Y.; Gong, S.; Zhang, X.; Henze, D. K.; Capps, S. L.; Fu, T. M.; Zhang, Q.; Wang, Y. Source  
520 attribution of particulate matter pollution over North China with the adjoint method. *Environ. Res. Let.* **2015**, *10* (8),  
521 084011.
- 522 (32) Heo, J.; Adams, P. J.; Gao, H. O. Public Health Costs of Primary PM<sub>2.5</sub> and Inorganic PM<sub>2.5</sub> Precursor Emissions in the  
523 United States. *Environ. Sci. Technol.* **2016**, *50* (11), 6061-6070.
- 524 (33) Wang, R.; Tao, S.; Shen, H.; Huang, Y.; Chen, H.; Balkanski, Y.; Boucher, O.; Ciais, P.; Shen, G.; Li, W.; Zhang, Y.;  
525 Chen, Y.; Lin, N.; Su, S.; Li, B.; Liu, J.; Liu, W. Trend in global black carbon emissions from 1960 to 2007. *Environ.*  
526 *Sci. Technol.* **2014**, *48* (12), 6780-6787.
- 527 (34) Huang, Y.; Shen, H.; Chen, H.; Wang, R.; Zhang, Y.; Su, S.; Chen, Y.; Lin, N.; Zhuo, S.; Zhong, Q.; Wang, X.; Liu, J.;

- 528 Li, B.; Liu, W.; Tao, S. Quantification of global primary emissions of PM<sub>2.5</sub>, PM<sub>10</sub>, and TSP from combustion and  
529 industrial process sources. *Environ. Sci. Technol.* **2014**, *48* (23), 13834-13843.
- 530 (35) Bell, M. L.; Dominici, F.; Ebisu, K.; Zeger, S. L.; Samet, J. M. Spatial and temporal variation in PM(2.5) chemical  
531 composition in the United States for health effects studies. *Environ. Health Perspect.* **2007**, *115* (7), 989-995.
- 532 (36) Pérez, N.; Pey, J.; Querol, X.; Alastuey, A.; López, J. M.; Viana, M. Partitioning of major and trace components in  
533 PM<sub>10</sub>-PM<sub>2.5</sub>-PM<sub>1</sub> at an urban site in Southern Europe. *Atmos. Environ.* **2008**, *42*, 1677-1691.
- 534 (37) Dawson, J. P.; Adams, P. J.; Pandis, S. N. Sensitivity of PM<sub>2.5</sub> to climate in the Eastern US: a modeling case study.  
535 *Atmos. Chem. Phys.* **2007**, *7*, 4295-4309.
- 536 (38) Jiménez-Guerrero, P.; Gomez-Navarro, J. J.; Jerez, S.; Lorente-Plazas, R.; Garcia-Valero, J. A.; Montavez, J. P.  
537 Isolating the effects of climate change in the variation of secondary inorganic aerosols (SIA) in Europe for the 21st  
538 century (1991–2100). *Atmos. Environ.* **2011**, *45* (4), 1059-1063.
- 539 (39) Du, C.; Liu, S.; Yu, X.; Li, X.; Chen, C.; Peng, Y.; Dong, Y.; Dong, Z.; Wang, F. Urban boundary layer height  
540 characteristics and relationship with particulate matter mass concentrations in Xi'an, central China. *Aerosol Air Qual.*  
541 *Res.* **2013**, *13* (5), 1598-1607.
- 542 (40) Tiwari, S.; Srivastava, A. K.; Bisht, D. S.; Parmita, P.; Srivastava, M. K.; Attri, S. D. Diurnal and seasonal variations of  
543 black carbon and PM<sub>2.5</sub> over New Delhi, India: Influence of meteorology. *Atmos. Res.* **2013**, *125-126*, 50-62.
- 544 (41) Shahsavani, A.; Naddafi, K.; Haghhighifard, N. J.; Mesdaghinia, A.; Yunesian, M.; Nabizadeh, R.; Arahami, M.; Sowlat,  
545 M. H.; Yarahmadi, M.; Saki, H.; Alimohamadi, M.; Nazmara, S.; Motevalian, S. A.; Goudarzi, G. The evaluation of  
546 PM<sub>10</sub>, PM<sub>2.5</sub>, and PM<sub>1</sub> concentrations during the Middle Eastern Dust (MED) events in Ahvaz, Iran, from april through  
547 september 2010. *J. Arid Environ.* **2012**, *77*, 72-83.
- 548 (42) Chen, H.; Huang, Y.; Shen, H.; Chen, Y.; Ru, M.; Chen, Y.; Lin, N.; Su, S.; Zhuo, S.; Zhong, Q.; Wang, X.; Liu, J.; Li,  
549 B.; Tao, S. Modeling temporal variations in global residential energy consumption and pollutant emissions. *Appl. Energ.*  
550 **2016**, *184*, 820-829.
- 551 (43) Suri, V.; Chapman, D. Economic growth, trade and energy: implications for the environmental Kuznets curve. *Ecol.*  
552 *Econ.* **1998**, *25*, 195-208.
- 553 (44) Zheng, M.; Salmon, L. G.; Schauer, J. J.; Zeng, L.; Kiang, C. S.; Zhang, Y.; Cass, G. R. Seasonal trends in PM<sub>2.5</sub> source  
554 contributions in Beijing, China. *Atmos. Environ.* **2005**, *39* (22), 3967-3976.
- 555 (45) Gao, J.; Woodward, A.; Vardoulakis, S.; Kovats, S.; Wilkinson, P.; Li, L.; Xu, L.; Li, J.; Yang, J.; Cao, L.; Liu, X.; Wu,  
556 H.; Liu, Q. Haze, public health and mitigation measures in China: A review of the current evidence for further policy  
557 response. *Sci. Total Environ.* **2017**, *578*, 148-157.
- 558 (46) Zheng, G. J.; Duan, F. K.; Su, H.; Ma, Y. L.; Cheng, Y.; Zheng, B.; Zhang, Q.; Huang, T.; Kimoto, T.; Chang, D.; Pöschl,  
559 U.; Cheng, Y. F.; He, K. B. Exploring the severe winter haze in Beijing: the impact of synoptic weather, regional  
560 transport and heterogeneous reactions. *Atmos. Chem. Phys.* **2015**, *15* (6), 2969-2983.
- 561 (47) Cai, W.; Li, K.; Liao, H.; Wang, H.; Wu, L. Weather conditions conducive to Beijing severe haze more frequent under  
562 climate change. *Nat. Clim. Change* **2017**, *7* (4), 257-262.
- 563 (48) Kelly, J.; Makar, P. A.; Plummer, D. A. Projections of mid-century summer air-quality for North America: effects of  
564 changes in climate and precursor emissions. *Atmos. Chem. Phys.* **2012**, *12* (12), 5367-5390.
- 565 (49) Tie, X.; Zhang, Q.; He, H.; Cao, J.; Han, S.; Gao, Y.; Li, X.; Jia, X. C. A budget analysis of the formation of haze in  
566 Beijing. *Atmos. Environ.* **2015**, *100*, 25-36.
- 567 (50) Hedegaard, G. B.; Christensen, J. H.; Brandt, J. The relative importance of impacts from climate change vs. emissions  
568 change on air pollution levels in the 21st century. *Atmos. Chem. Phys.* **2013**, *13* (7), 3569-3585.
- 569 (51) Pey, J.; Querol, X.; Alastuey, A.; Forastiere, F.; Stafoggia, M. African dust outbreaks over the Mediterranean Basin  
570 during 2001-2011: PM<sub>10</sub> concentrations, phenomenology and trends, and its relation with synoptic and mesoscale  
571 meteorology. *Atmos. Chem. Phys.* **2013**, *13* (3), 1395-1410.
- 572 (52) Riahi, K.; Grübler, A.; Nakicenovic, N. Scenarios of long-term socio-economic and environmental development under



- 573 climate stabilization. *Technol. Forecast. Soc.* **2007**, *74* (7), 887-935.
- 574 (53) van Vuuren, D. P.; den Elzen, M. G. J.; Lucas, P. L.; Eickhout, B.; Strengers, B. J.; van Ruijven, B.; Wonink, S.; van  
575 Houdt, R. Stabilizing greenhouse gas concentrations at low levels: an assessment of reduction strategies and costs.  
576 *Climatic Change* **2007**, *81* (2), 119-159.
- 577 (54) Mansha, M.; Ghauri, B.; Rahman, S.; Amman, A. Characterization and source apportionment of ambient air particulate  
578 matter (PM<sub>2.5</sub>) in Karachi. *Sci. Total Environ.* **2012**, *425*, 176-183.
- 579 (55) Li, C.; McLinden, C.; Fioletov, V.; Krotkov, N.; Carn, S.; Joiner, J.; Streets, D.; He, H.; Ren, X.; Li, Z.; Dickerson, R. R.  
580 India Is Overtaking China as the World's Largest Emitter of Anthropogenic Sulfur Dioxide. *Sci. Rep.* **2017**, *7*, 14304.